ACS OMEGA

Open Access

http://pubs.acs.org/journal/acsodf

Article

Research on the Resourceful and Efficient Recycling Technology of Waste Thermal Insulation Pipe Material

Xiaohua Gu,* Qinglong Zhao, Shangwen Zhu, Yan Liu, and Qingyong Su

Cite This: *ACS Omega* 2025, 10, 12917−12927

Read Online

ACCESS | Metrics & More | Article Recommendations | Supporting Information

ABSTRACT: This study was conducted to explore a new method for degrading and recycling waste chemical pipe insulation and cooling materials. A chemical degradation method was employed, utilizing alkali metal catalysts and a two-component alcoholysis system consisting of specific ratios of diethylene glycol and butylene glycol. The system effectively degraded the polyisocyanurate (PIR) insulation with the aim of reusing the waste material. The experimental results show that the best reaction performance is obtained with 1,4-BG/DEG ratio of 43:57 at 180 and 190 °C 1 h. The resulting regenerated pipe has an apparent density of 0.041 g/cm^3 and a compressive strength of 0.413 MPa. With remarkable thermal stability, well-preserved porosity, and strong skeletal structure, the cold loss on the outer surface of the insulated pipe is lower than the design requirement of 23 W/m^2, which is qualified for the energy efficiency of the insulated pipe. The proposed strategy for degradation and recycling of waste chemical pipe insulation and cold insulation materials provides a pioneering green treatment method for the task of recycling polyurethane waste with fire-resistant degradability and a high cross-linking degree.

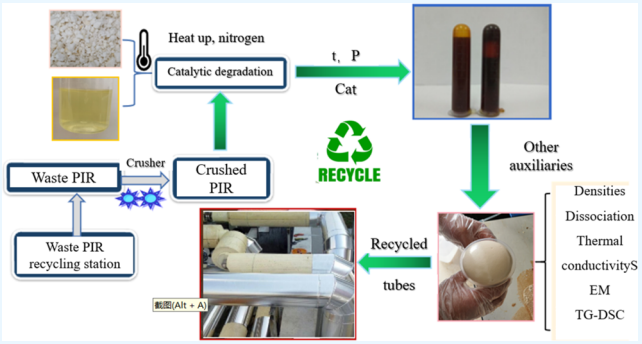

1. INTRODUCTION

Polyurethane rigid foam, commonly referred to as PUR foam, boasts an impressive array of features that include superior thermal insulation, lightweight construction, high specific strength, exceptional chemical resistance, and notable soundproofing effects. As a vital type of synthetic resin insulation material, it finds extensive application across diverse thermal insulation scenarios in industries such as construction, petrochemicals, refrigeration, and more.[1−3] The widespread adoption of PUR foam is underpinned by its diverse applications and soaring market demand.[4−6] Within this realm, polyisocyanurate, abbreviated as PIR, also known as "polyisocyanate foam PIR" or simply "polyester PIR", stands out as a novel cryogenic insulation material suitable for use within a broad temperature range of −196 to +120 °C. PIR foam combines urethane groups with polyisocyanurate groups, where the latter's distinctive six-membered isocyanurate ring structure arises from the trimerization of excess isocyanate molecules during the foaming process.[7] This unique structure contributes to a higher cross-linking network, low thermal conductivity, and exceptional thermal stability compared to PUR foam.[8] PIR not only excels in thermal properties but also demonstrates remarkable fire performance, typically achieving a B2 rating. By fine-tuning the concentration of polyisocyanurate rings and adopting advanced formulation techniques, it can even attain a B1 rating with an oxygen index exceeding 35%.[9] As an ideal organic insulation material, PIR boasts low thermal conductivity, robust weather resistance, and the flexibility to be prefabricated or poured onsite. These advantages make PIR an ideal choice for cryogenic insulation in pipelines of oil refineries, chemical plants, ethylene, fertilizer, and other industries.

Amidst the rapid advancements in the polyurethane industry, global consumption of polyurethane is projected to escalate annually over the upcoming years, averaging a growth rate of approximately 6.7% per annum.[10−13] China's polyurethane sector, which embarked on its journey in the late 1950s, witnessed gradual progress, particularly with the introduction and establishment of raw material facilities like isocyanate MDI.[14−17] Since then, the industry has accelerated its pace, though early disposal methods for PIR and polyurethane waste, such as landfilling and incineration,[18−21] resulted in severe pollution and resource wastage.[22−26] Consequently, the adoption of chemical recycling and degradation processes to derive novel recycled materials not only mitigates resource depletion but also addresses environmental pollution concerns, thereby presenting a promising future for the PIR and polyurethane waste degradation industries.[27−29]

Received: September 10, 2024
Revised: January 20, 2025
Accepted: January 21, 2025
Published: March 24, 2025

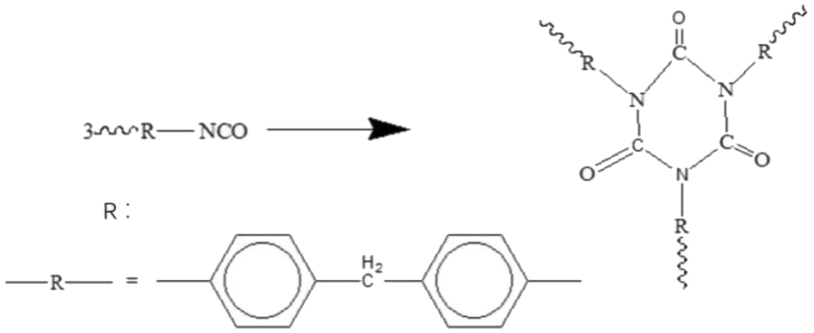

Figure 1. Schematic diagram of the PIR structure.

This paper delves into the utilization of a two-component alcoholic agent, facilitated by an alkali metal catalyst, for the recovery of thermal and cold insulation materials from waste chemical pipelines. Figure 1 shows the structure of the PIR. Through rigorous experimentation, the degradation conditions of waste PIR were meticulously analyzed, culminating in the identification of optimal degradation parameters. Alcoholysis regenerates PIR with a yield of 80−90% and a purity of more than 90%, while PIR degraded by other means tends to have a yield of 70% and a purity of about 60%. This innovative approach offers a fresh perspective and an efficient means for the chemical recycling of waste polyurethane, opening new avenues for sustainable waste management.

2. EXPERIMENTAL PART

2.1. Main Raw Materials. PIR Waste (Tianjin Petrochemical), Diethylene Glycol (AR, Fuchen Chemical), Butylene Glycol (AR, Fuchen Chemical), Potassium Hydroxide (99.9%, McClean), Combined Polyether Polyol (Bluestar Dongda), polyisocyanate (Wuhan Huaxiang Kejie Biotechnology Co., Ltd.), dimethicone DSO (99.9%, Jinan Haiyuan Chemical Co., Ltd.), 1-fluoro-1,1-dichloroethane HCFC-141b (99.9%, Jinan Haiyuan Chemical Co., Ltd.), triethanolamine (99.9%, McClean), and dibutyltin dilaurate (99.9%, Jinan Haiyuan Chemical Co., Ltd.). Waste PIR is the key to this study and its microstructure. The waste PIR microscopic image is shown in Figure 2.

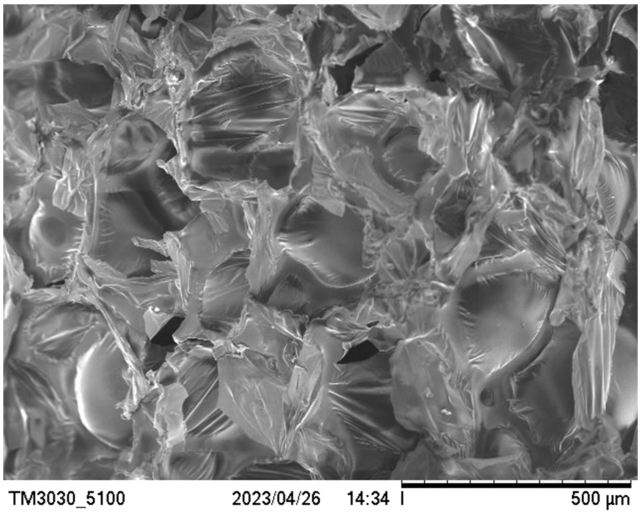

Figure 2. Waste PIR microstructure diagram.

Also, some of the properties of used PIRs are as follows: density: 0.312 cm^3/g, thermal conductivity: 0.025 W/(m·K), compressive strength: 0.317 MPa.

2.2. Experimental methods. *2.2.1. Waste PIR Alcoholysis Experiment.* Alcoholysis solvents are crucial in the alcoholysis reaction of PIR foams, as they dissolve the reactants and facilitate the reaction. In order to avoid excessive byproducts affecting product quality, this paper adopts the experimentally verified optimal ratio, i.e., the mass ratio of the alcoholysis solvent to the PIR foam, to ensure that there is no large amount of excess solvent, so as to balance the reaction rate and the cost of subsequent treatment. From a techno-economic point of view, the solvent cost affects the production cost, so the optimized solvent ratio used in this paper aims to improve the reaction selectivity and yield. Specifically, a mixture of 100 g of 1,4-BG and DEG, in equal proportions, was introduced into the reactor as the alcoholytic agent, along with a 1% (0.6 g) alkali metal catalyst (AMC). Subsequently, 100 g of waste PIR powder(See Figure S1) was added, and the mixture was subjected to stirring alcoholysis at 180 °C for 2 h, resulting in the successful synthesis of the alcoholized material.

The waste PIR was first segmented into smaller pieces and processed through a crusher to achieve a fine powder form. This powder was then introduced into the reaction kettle. For the degradation process, a two-component alcoholytic agent consisting of butylene glycol (1,4-BG) and diethylene glycol (DEG) combined in varying proportions was utilized. Specifically, 100 g of this agent, along with 10 g of alkali metal catalyst (AMC), were added to the kettle. The preweighed waste polyurethane powder was subsequently incorporated into the mixture. The system was continuously heated to 180 °C, maintained at this temperature for 1 h, and then further increased to 190 °C for an additional hour to complete the reaction. This process yielded the regenerated polyol (RP), which underwent subsequent testing, analysis, and foaming procedures. The two-component alcoholytic agent effectively catalyzed the degradation of the waste PIR, and Figure 3 illustrates the underlying degradation reaction mechanism.

Under the catalytic influence of AMC and at elevated temperatures within the reaction kettle, 1,4-BG and DEG function as efficient alcoholytic agents. This results in the cleavage of the polyisocyanurate urea bonds within the waste PIR, which are subsequently replaced by alcoholytic agents to generate polyester polyols. The intricate reaction mechanism underlying this process is visually depicted in Figure 3.

2.2.2. Preparation of Thermal Insulation and Cold Insulation Materials for Recycled New Chemical Pipelines. The degraded recycled polyether polyol 7 g of RP, 23 g of

https://doi.org/10.1021/acsomega.4c07807
ACS Omega 2025, 10, 12917−12927

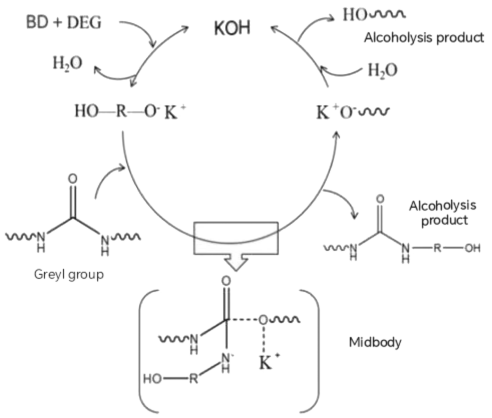

Figure 3. Schematic diagram of the degradation mechanism of waste PIR by the AMC catalyst.

commercial polyether polyol 4110, 2.5 g of dimethyl silicone oil, 13g of foaming agent (CAS 287-92-3), 0.3 g of catalyst triethanolamine, and 0.1 g of dibutyltin dilaurate were added to disposable plastic cups and stirred with a cantilever mixer, and the stirring time was 2 min. Then 45 g of polyisocyanate is added to the well-mixed product, and stirring will continue to prepare the foaming material. The prepared new chemical pipeline materials were allowed to stand in a cool and dry place for 24 h, and samples were made according to the test standards. Therefore, the schematic diagram of the green recycling process of degrading waste PIR is shown in Figure 4.

2.2.3. Polyurethane Performance Testing and Characterization. 2.2.3.1. Viscosity Test. To conduct the viscosity test of the degradation products at 43 °C, the sample bottle containing the degradation product is carefully positioned directly beneath the viscosity tester probe,[30] ensuring that the probe does not penetrate the sample (avoiding contact with the bottle's bottom). The viscosity measurement is then performed, with meticulous attention paid to recording the rotor type, rotational speed, viscosity readings (in 5 separate groups), and the corresponding opening angles (in 5 separate groups) for accurate analysis.

2.2.3.2. Hydroxyl Value Test. An appropriate amount of degradation products is placed in an Erlenmeyer flask, and the hydroxyl value is determined by the pyridine method according to the GB/T12008.3-2009 standard.[31]

2.2.3.3. FTIR Spectroscopy. At ambient temperature, the structural composition of the degradation products was verified through infrared spectroscopy using a Spectrum-One FTIR spectrometer manufactured by PE in the United States.[32] The spectral range was set between 4000 and 500 cm^{-1} to capture a comprehensive view of the molecular features. Prior to analysis, an appropriate quantity of the degradation product specimens underwent drying and subsequent waste chemical pipe insulation and cooling material (NCPM) procedures. Fourier transform infrared spectroscopy was employed to analyze the structure of the samples, providing insights into their chemical makeup.

2.2.3.4. Apparent Density Test. The apparent density of the recycled polyurethane foam is rigorously tested in accordance with the nationally recognized standard GB/T6343-2009.[33] To ensure accuracy, the foam, after standing for 24 h to attain stability, is precisely cut into sample blocks. Each sample block undergoes a rigorous weighing process with five individual measurements taken and their average calculated to determine the definitive weight of the block. Subsequently, the apparent density was calculated using below formula, ensuring that the final result adheres to the highest standards of accuracy and precision.

$$\rho = m/v$$

ρ − Object density, g/cm^3, m − Mass of the object, g, v-The volume of the object,cm^3. The density of the recycled polyurethane foam is calculated.

2.2.3.5. Compressive Strength Test. Adhering to the GB-8813-88 test standard, a universal testing machine is utilized to assess the strength of carefully dimensioned test blocks.[34] During the test, the compression velocity of the machine is carefully controlled, and the compression deformation of each test block is meticulously recorded. To ensure reliability, the average of all test results is calculated and adopted as the

Figure 4. Schematic diagram of the green recycling process of degrading waste PIR.

https://doi.org/10.1021/acsomega.4c07807
ACS Omega 2025, 10, 12917−12927

compressive strength representative of each group of test blocks. Furthermore, this compressive strength is analyzed and compared against that of a pure sample, with a known compressive strength of 240 Pa, to provide valuable insights into the performance of the recycled material.

2.2.3.6. Thermogravimetric (TG) Analysis. Employing a thermogravimetric analyzer, the experimental sample was subjected to a temperature ramp from room temperature (25 °C) to 800 °C, within a nitrogen atmosphere, at a controlled heating rate of 10 °C/min. During this process, air served as the carrier gas, flowing at a steady rate of 50 mL/min. Alumina was utilized as the reference material to facilitate accurate thermogravimetric analysis. Following the completion of the experiment, the acquired data were meticulously sorted and analyzed to gain insights into the thermal stability and degradation behavior of the sample.

2.2.3.7. Scanning Electron Microscopy. Sections of new chemical pipeline materials and then placing the slices on the stage for vacuuming and gold spraying.[35] The skeleton and cell structure of each NCPM specimen were observed by using mirrors of different magnifications.

2.2.3.8. Thermal Conductivity Test. Conforming to the GB/T10294-2008 standard, the thermal conductivity of novel chemical pipeline materials is rigorously assessed using the QTM-500 thermal conductivity analyzer.[36] To ensure precision, each proportionally prepared sample undergoes testing three times, and the average of these measurements is adopted as the final result. The test parameters are carefully set, with a duration of 160 s, a sampling interval of 640 ms, a test power of 0.17 W, and the thermal conductivity unit expressed as W/(m·K), providing a comprehensive and accurate assessment of the material's thermal properties.

2.2.3.9. Thermal Insulation Test. The recycled PIR pipe shell of Φ219 was applied to the electric heating pipe of Φ219, and the temperature of the pipe was raised to 60 and 100 °C, respectively. After the temperature is stable and the steady-state heat transfer is reached, the ambient temperature is tested with a Testo-925 temperature tester, and the outer surface temperature and outer surface heat flux of the PIR are measured by the HFM-201 heat flux meter.

3. RESULTS AND DISCUSSION

3.1. Hydroxyl Value and Viscosity Analysis of Regenerated Polyol (RP). Figure 5 presents the comprehensive characterization results of the hydroxyl number and viscosity of the recycled polyol (RP) (see Figure S2) derived from the degradation of waste polyurethane using varying proportions of a two-component alcoholytic agent (1,4-BG:DEG). Notably, the RP exhibits a hydroxyl value (420) and viscosity that closely resemble those of commercially available (pure) polyether polyol 4110, indicating the effectiveness of the two-component alcoholytic agent in catalyzing the complete degradation of waste polyurethane. Furthermore, the RP recovered through the use of alkali metal catalyst (AMC) catalysts demonstrates a superior hydroxyl value compared to traditional degradation methods, attributable to the enhanced catalytic activity of these metals. Intriguingly, as the proportion of 1,4-BG in the alcoholytic agent gradually increases, the hydroxyl value of the RP initially rises and then declines. This trend can be explained by the corresponding change in viscosity of the regenerated polyol, which initially decreases and subsequently increases with the 1,4-BG content. Optimally, when the 1,4-BG:DEG ratio is

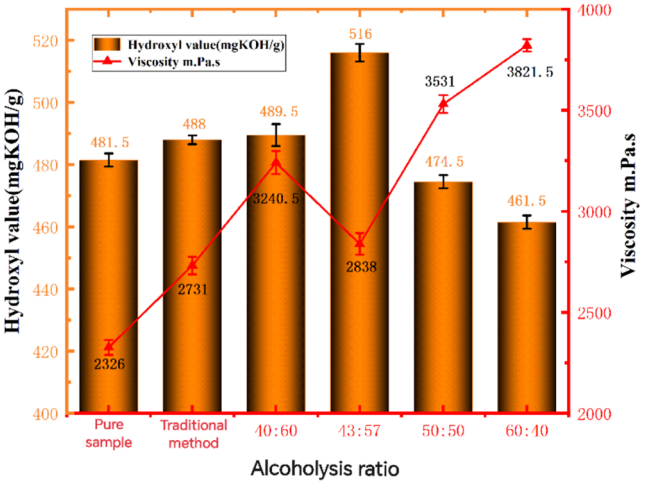

Figure 5. Hydroxyl value and viscosity analysis of RP.

43:57, the degradation process yields the highest hydroxyl value of 512 KOH/g alongside the lowest viscosity of 2876 mPa·s. This optimal condition results in a degradation product that boasts exceptional performance and fluidity, making it highly suitable for various applications.

3.2. Infrared Spectroscopy Analysis of Regenerated Polyether Polyols of Degradation Products. The IR spectral analyses of RP and commercially available polyester polyols, both prepared with equal amounts of AMC, revealed interesting similarities and differences in their spectral characteristics.[37−39] As shown in Figures 6 and 7, the RP

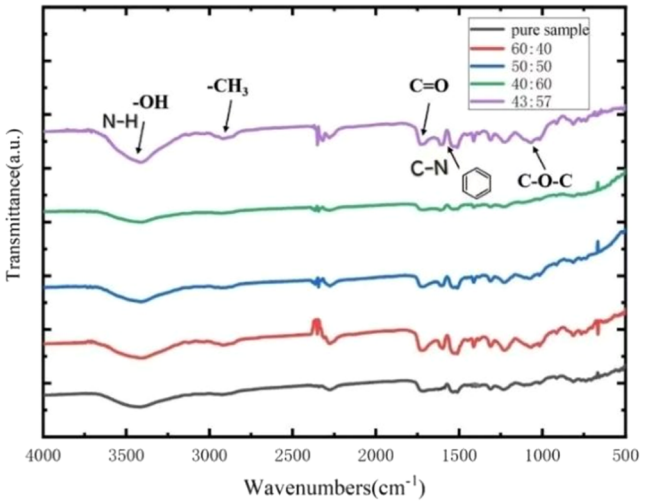

Figure 6. Infrared spectra of the regenerated polyols.

samples exhibited characteristic peaks almost identical to those of the commercially available polyester polyols irrespective of the type and proportion of the alcohol solvent used, suggesting that the effect of the alcohol solvent composition is minimal. The peak at about 2300 cm^{-1} in Figure 6 is identical to the isocyanic acid N═C═O stretching band typically observed at 2270−2280 cm^{-1}. The N−H in-plane bending vibration of the regenerated polyether polyol containing urethane groups (amide II band) is observed at 1508 cm^{-1}. At wave numbers of 1500−1560 cm^{-1}, it has been shown to be the characteristic peak range of linear aromatic benzene rings. The C−N stretching vibrations of regenerated polyether polyols are

https://doi.org/10.1021/acsomega.4c07807
ACS Omega 2025, 10, 12917−12927

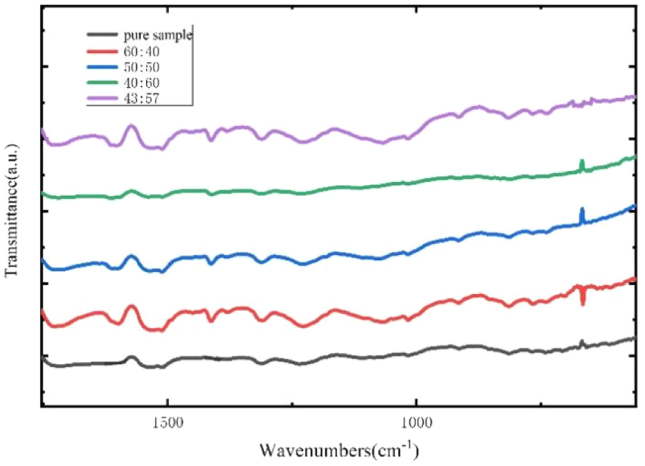

Figure 7. Infrared spectra with partial enlargement.

present at around 1530−1540 cm^{-1}. The sharp band at 1412−1410 cm^{-1} is typical of the C−N stretching vibrations of isocyanurate rings. The Ar−H deformation of the aryl ring is found at about 1590 cm^{-1}. N−H stretching is present in the 3500−3300 cm^{-1} range; the 2900 cm^{-1} band is typical not only of methyl groups but also of various alkyl groups. The prominent stretching vibrational peak centered at 3350 cm^{-1} indicates the presence of alcohol hydroxyl (−OH), while the characteristic absorption peaks at 2900 and 1737 cm^{-1} correspond to methyl and carbonyl groups, respectively. These findings suggest that the urea bonds of polyisocyanurates are efficiently broken and replaced by alcohol hydroxyl groups under the alcoholysis of discarded PIR foams, resulting in regenerated polyol blends rich in ether bonds.[40] This structural similarity to commercial polyester polyols emphasizes the potential of RP in the preparation of regenerated polyurethane PIR foams, providing a sustainable alternative to conventional materials.

3.3. Analysis of Apparent Density of Recycled Cold Insulation Materials. The analysis of the apparent density of NCPMs prepared using a two-component alcoholytic agent with varying proportions of butylene glycol (1,4-BG) and diethylene glycol (DEG) reveals an intriguing trend as depicted in Figure 8. As the proportion of 1,4-BG gradually increases, the apparent density initially rises and subsequently declines, likely attributed to the evolving interactions between these two components. Butylene glycol, being a highly polar and relatively high-molecular-weight organic compound, exhibits strong intermolecular interactions with diethylene glycol. At low 1,4-BG concentrations, these interactions are sparse, contributing to a lower overall apparent density. However, as 1,4-BG content increases, the intensification of molecular interactions − encompassing hydrogen bonds and van der Waals forces − leads to a corresponding rise in apparent density. Paradoxically, when 1,4-BG levels surpass a certain threshold, the excessive amount of butylene glycol introduces more free volume within the system, counteracting the density-enhancing effects of stronger interactions. Additionally, high 1,4-BG concentrations may disrupt the orderly arrangement of molecules, further contributing to a decrease in apparent density. Remarkably, all AMC-catalyzed NCPMs (Figure S1) exhibit higher apparent densities than their pure counterparts, with the peak density (0.041 g/cm^3) observed at a 1,4-BG:DEG ratio of 43:57. This indicates that under this

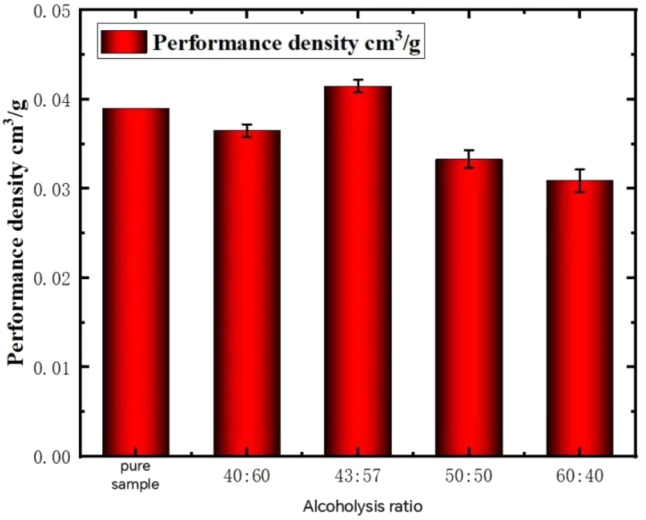

Figure 8. Analysis of the performance density of cold insulation materials.

specific composition, the NCPM possesses a more compact internal structure, maximizing density within the same volume. Moreover, all of the regenerated foams and pure samples had higher densities than the spent PIR, suggesting that solid waste regeneration can reductively improve the performance of the spent PIR that has been degraded by aging.

3.4. Analysis of Compressive Strength of Recycled Cold Insulation Materials. Figure 9 depicts the compressive

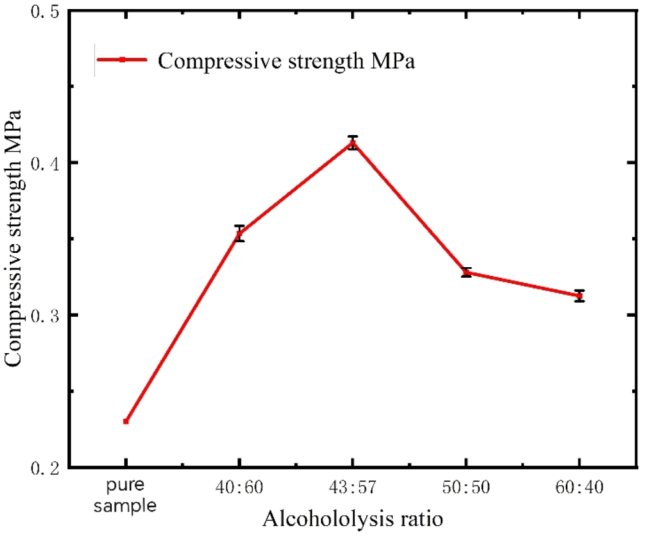

Figure 9. Analysis of compressive strength of cold insulation materials.

strength of NCPM and its pure counterpart, revealing a clear trend: as the quantity of 1,4-BG gradually increases, the compressive strength initially escalates and subsequently declines. This trend aligns perfectly with the variation observed in the density of the material. Denser NCPMs exhibit a tighter internal structure and fortified intermolecular forces, which in turn contribute to an enhanced compressive strength. Notably, at a 1,4-BG:DEG ratio of 43:57, the NCPM achieves its peak compressive strength of 0.413 MPa, marking the optimal performance in this regard and correlating well with its heightened density. Moreover, the compressive strength of the

https://doi.org/10.1021/acsomega.4c07807
ACS Omega 2025, 10, 12917−12927

recycled foam was higher than that of the spent foam in all proportions except for the pure sample. This suggests that recycled foam retains the compressive strength of polyurethane while also being of solid waste recycling significance.

3.5. Test and Analysis of Thermal Conductivity of Recycled Cold Insulation Materials. The analysis of the thermal conductivity of regenerated polyisocyanurate (PIR) at room temperature was conducted in a laboratory setting utilizing the QTM-500 thermal conductivity tester. The results, as depicted in Figure 10, demonstrate that the thermal

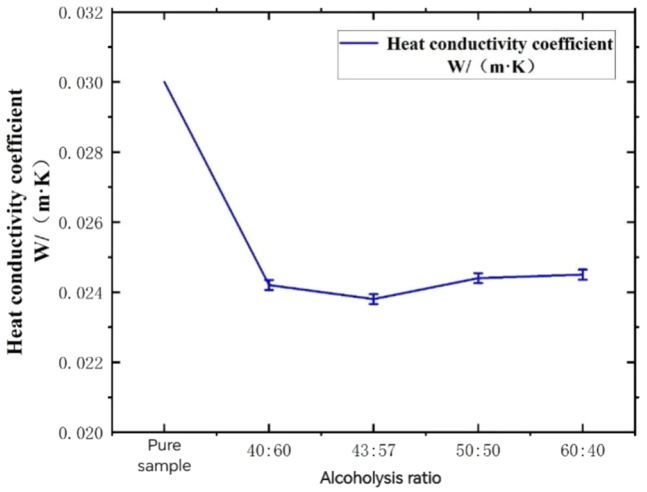

Figure 10. Recycled PIR tube shell test diagram of thermal conductivity at room temperature.

conductivity of the regenerated PIR at room temperature is 0.0239 W/(m·K), which is the lowest recorded value and thus indicates the superior insulation performance. Notably, this value surpasses that of pure PIR, which is 0.030 W/(m·K), underscoring the enhanced thermal properties of the regenerated material. The improved thermal conductivity can be attributed to the unique molecular structure of the degradation products, which retain the rigid benzene ring structure of the black material found in the original waste PIR. This, combined with the rigid cell structure achieved through the foaming and regeneration processes, results in a material that is less prone to cell collapse. As a closed-cell material, the regenerated PIR boasts more stable and uniform cells, effectively impeding heat transfer and enhancing its insulation capabilities. The thermal conductivity of the waste foam is reduced due to time, and the thermal conductivity of the recycled foam is higher than that of the waste foam in all cases compared to that of the recycled foam.

3.6. Analysis of Thermal Loss (TG) of Recycled Cold Insulation Materials. The thermogravimetric analysis of NCPM derived from the alcoholysis of various two-component alcoholytic agents reveals a distinct three-stage weight loss pattern. As shown in Figure 11, The initial stage, spanning 100−200 °C, primarily corresponds to the evaporation of free and bound water within the foam, though this is often inconspicuous due to the foam's inherently low free water content.[41−43] The second stage, occurring between 200−390 °C, marks the decomposition of the hard segment in the PIR foam, encompassing structural units formed by isocyanates and aromatics. This decomposition rate peaks approximately at 310 °C. The third stage, ranging from 390−780 °C, represents the fracturing of the polyester soft segment within the PIR,

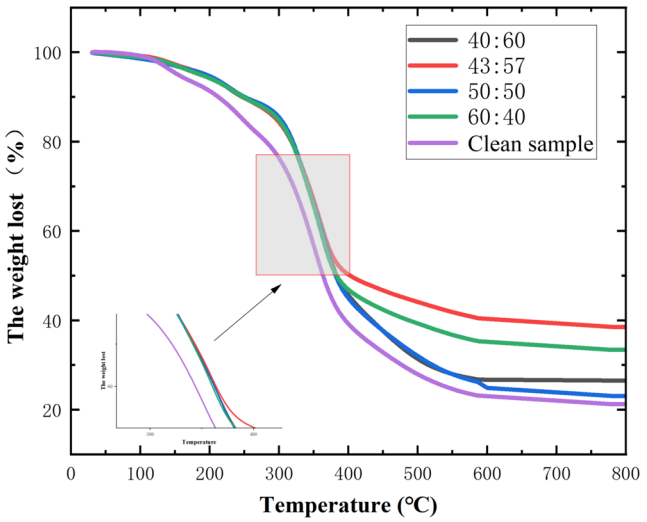

Figure 11. Thermogravimetric (TG) diagram of recycled cold insulation material.

featuring aliphatic polyester-based structural units.[44−46] Notably, the significant weight loss for NCPM prepared using different proportions of alcoholytic agents occurs around 250 °C, with decomposition ceasing at approximately 780 °C. Interestingly, the pure sample and NCPM prepared with a 1,4-BG:DEG ratio of 43:57 exhibit a maximum decomposition rate at approximately 338 and 350 °C, respectively. This indicates that the foam in the latter group, derived from degradable materials, possesses greater chemical bond energy, translating into superior high-temperature resistance compared to other NCPM samples obtained through alcoholysis. Furthermore, the thermal stability of NCPM prepared as a degradable material, sourced from the degradation and recycling of waste PIR, is comparable to or even superior to that of pure samples. This underscores the enhanced stability and improved resilience of polyurethane foam to environmental fluctuations during practical applications, demonstrating the effectiveness of the recycling and degradation process in enhancing the overall performance of NCPM. As can be seen from Figure 12, the regenerated PIR foam has better high-temperature resistance when the ratio of alcohol solvent is 43:47, which

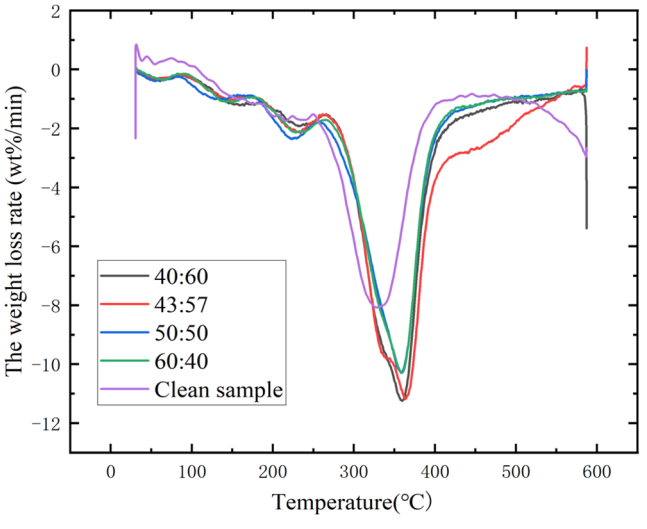

Figure 12. Differential scanning calorimetry(DSC) diagram.

https://doi.org/10.1021/acsomega.4c07807
ACS Omega 2025, 10, 12917−12927

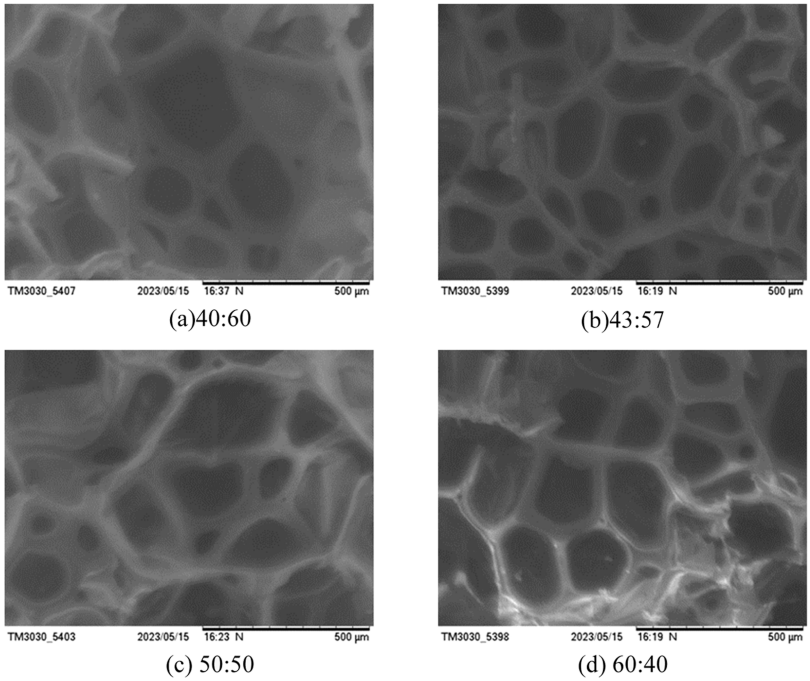

Figure 13. Scanning electron microscopy (SEM) of cold insulation material.

corresponds to the TG data in Figure 11, further indicating that the regenerated PIR has good.

3.7. Scanning Electron Microscopy Analysis of Recycled Cold Insulation Materials. Scanning Electron Microscopy(SEM) analysis serves as a crucial and multifaceted tool for examining foam morphology, providing valuable insights into the efficacy of bubble growth within the intricate network of tightly arranged bubbles that collectively constitute the characteristic honeycomb structure of foam.[47,48] By analyzing NCPM sample sections obtained through hydrolysis with various two-component alcoholytic agents, we conducted a meticulous observation, focusing on a distinct, clearly defined area for SEM photography. The resulting images, presented in Figure 13, vividly reveal the pore structure of each sample, offering a microscopic glimpse into the intricate foam architecture.

As depicted in Figure 13, the NCPMs synthesized using varying 1,4-BG:DEG ratios of 40:60, 50:50, and 60:40 exhibit distinct cell sizes, with the SEM images revealing varying degrees of cell disruption or fragmentation. Compared with Figure 2, all the regenerated PIR pore structures are better than the used PIR, and the skeletons are relatively thicker, which indicates that the microscopic properties of the regenerated PIR are better than those of the used PIR. Notably, the NCPM prepared with a 1,4-BG:DEG ratio of 43:57 stands out for its full and regular polygon-shaped cells, accompanied by a significant reduction in cell junction ruptures. This sample boasts thicker pore walls, translating into enhanced foam performance and thermal insulation capabilities. The underlying mechanism can be attributed to the optimal balance achieved by the 1,4-BG:DEG ratio. As the proportion of 1,4-BG gradually increases, the waste polyurethane undergoes more effective urea bond cleavage during recovery and degradation processes. However, when 1,4-BG levels exceed a certain threshold, an "excessive" fracturing of urea bonds occurs. These excessively fragmented short segments subsequently undergo further breakage, yielding a heterogeneous mixture of chain lengths. This, in turn, leads to an uneven molecular weight distribution within the NCPM, resulting in severe cell fragmentation, compromised cell junction integrity, and a subsequent decline in foam strength and thermal insulation performance.[46,49−51] Therefore, the optimal 1,4-BG:DEG ratio of 43:57 represents a sweet spot that maximizes the beneficial effects while minimizing the detrimental consequences of urea bond cleavage.

3.8. Thermal Conductivity Test and Analysis. For the thermal conductivity analysis of regenerated PIR at room temperature, the thermal conductivity of PIR at room temperature was tested by the QTM-500 thermal conductivity tester in the laboratory, and the thermal conductivity test data of regenerated PIR are shown in Table 1. As can be seen from the table, the thermal conductivity of regenerated PIR is 0.0239 W/(m·K) when T_m is 20.8 °C. The thermal conductivity of recycled PIR at room temperature was better than that of pure PIR = 0.030 W/(m·K). This is because the small molecular chain of the degradation product carries the rigid structure of the benzene ring of the black material in the original waste PIR, and the cell structure after foaming and regeneration is more rigid, and the cell structure is not easy to

Table 1. Thermal Conductivity Test Data of Recycled PIR Tube Shell at Room Temperature

serial number	T_m, °C	λ, W/(m·K)
1	20	0.0243
2	21	0.0234
3	21	0.0239
4	21	0.0241
5	21	0.0241
6	21	0.0242
7	21	0.0241
8	21	0.0242
average	20.8	0.0239

https://doi.org/10.1021/acsomega.4c07807
ACS Omega 2025, 10, 12917−12927

collapse. As a closed-cell material, more stable and uniform cells can effectively reduce heat transfer.

3.9. Regenerative PIR Adiabatic Effect. The recycled PIR pipe shell of Φ219 and sample PIR shell was applied to the electric heating pipe of Φ219, and the temperature of the pipe was raised to 60 and 100 °C, respectively. After the temperature is stable and the steady-state heat transfer is reached, the ambient temperature is tested with the Testo-925 temperature tester, and the outer surface temperature and outer surface heat flux of the PIR are measured by the HFM-201 heat flux meter. The test data are listed in Tables 2 and 3.

Table 2. Experimental Data on the Adiabatic Effect of Recycled PIR Tube Shells

serial number	medium temperature, °C	ambient temperature, °C	exterior surface temperature, °C	outer surface heat flux, W/m^2
1	60	16.5	19.3	23.6
2		16.8	19.9	22.7
3		16.6	19.7	25.1
average	60	16.6	19.6	23.8
1	100	17.6	23.3	50.4
2		17.4	234	50.0
3		17.5	23.5	50.0
average	100	17.5	23.4	50.1

Table 3. Experimental Data on the Adiabatic Effect of Pure Sample PIR Tube Shells

serial number	medium temperature, °C	ambient temperature, °C	exterior surface temperature, °C	outer surface heat flux, W/m^2
1	60	16.0	18.8	23.7
2		15.7	18.9	25.6
3		15.9	18.8	22.7
average	60	15.9	18.9	24.0
1	100	16.1	23.1	53.8
2		16.3	21.2	52.0
3		16.3	22.0	53.1
average	100	16.2	22.1	53.0

Based on the laboratory thermal test data and the calculation of Fourier's heat transfer law, λ = 0.037 W/(m·K) at T_m = 39.8 °C and λ = 0.041 W/(m·K) at T_m = 61.7 °C. λ = 0.037 W/(m·K) at T_m = 39.4 °C and λ = 0.043 W/(m·K) at T_m = 61.1 °C. The thermal insulation effect of recycled PIR shells is similar to or better than that of pure PIR shells. The insulating effect of regenerated PIR shells is similar to or better than that of pure sample PIR shells.

3.10. Evaluation of the Effectiveness of Industrial Applications. In order to further verify the evaluation of the effect of regenerated PIR pipe shells in practical application, the application of degradation of regenerated PIR pipe size Φ219 (See Figure S3) shells to replace the old cold-keeping layer of the renovation project of the actual application of the cold-keeping pipeline before and after the inlet line of the connecting pipeline to carry out the evaluation of the energy efficiency of the cold-keeping.The modifications are shown in Figure 14. And to this end, the regenerated pipe shell material in accordance with the size of the Φ219 shells after the preparation and get the results of the evaluation of the test as shown in Table 4.

The application of degradation and regeneration of PIR pipe shells to replace the old cold-keeping layer is practically applied in the remodeling project, and the temperature drop on the outer surface of the cold-keeping layer before and after the inlet line of the connection line of the shell with the cold-keeping pipeline size of Φ219 has been reduced by 3 °C; The cold loss on the outer surface was reduced by 20.21 W/m^2 respectively; after the transformation, the post-transformation test and cold-keeping energy efficiency evaluation were carried out, and the cold loss on the outer surface of the cold-keeping pipeline was lower than the design requirement of 23 W/m^2, and the performance of cold-keeping energy efficiency was qualified (See Figure S4).

4. CONCLUSIONS

In this comprehensive study, we successfully harnessed the synergy between an alkali metal catalyst (AMC) and a strategic blend of 1,4-butanediol and diethylene glycol in varying proportions to efficiently degrade and recover waste polyisocyanurate (PIR) foam. By meticulously analyzing the degradation conditions of the waste PIR, we identified the optimal ratio of these alcoholytic agents to facilitate the production of high-quality recycled polyols. The key findings of our investigation are summarized as follows:

(1) In the degradation of waste polyisocyanurate (PIR) foams using a two-component alcoholysis blend, the optimum mass ratio of 1,4-butanediol to diethylene glycol was determined to be 43:57 and 1% g of potassium hydroxide was added as a catalyst. The alcoholysis process was reacted at 180 °C for 1 h. After 1 h, the temperature was raised to 190 °C and the reaction was continued for 1 h. The alcoholysis conditions could be achieved to ensure the successful degradation of the waste PIR foams.

(2) The viscosity of the degradation product was 2876 m·Pa·s, and the compressive strength of the PIR foam

(a) Φ219 recycled tube shell

(b) Φ219 recycled pipe shell engineering installation application

Figure 14. Φ219 recycled tube shell engineering application test.

https://doi.org/10.1021/acsomega.4c07807
ACS Omega 2025, 10, 12917−12927

Table 4. Test and Evaluation Results after Modification of the Inlet Line of the Insulated Cold Connection Pipe

pipeline	pipe diameter mm	medium temp, °C	test time	cold insulation	insulation thickness, mm	cold loss on the outer surface of the original pipe, W/m^2	cold loss on the outer surface of new piping, W/m^2	temp drop of the outer surface of the original pipeline, °C	outer surface temperature drop, °C	keep cold energy efficiency
connect the pipeline	Φ219	−14	after remodel	regenerate PIR	60	28.4	8.19	4	1	qualified

obtained by foaming and regeneration of the degradation product was 0.413 MPa, the apparent density was 0.041 g/cm^3 and the thermal conductivity was 0.0239 W/(m·K), all of which were better than the pure PIR foam materials. Moreover, before and after the actual application of the connecting pipeline inlet pipeline with the size of Φ219 pipe shell, the temperature drop on the outer surface of the cold-insulating layer was reduced by 3 °C; the cold loss on the outer surface was reduced by 20.21 W/m^2 respectively, and the cold loss on the outer surface of the cold-insulating pipeline was lower than the design requirement of 23 W/m^2, and the cold-insulating energy efficiency was qualified.

(3) The new type of chemical pipeline thermal insulation and cold insulation material successfully prepared meets the national standard, the sample bubble hole is relatively complete, the skeleton is relatively thick and the thermal insulation effect is good to achieve the best performance.

Nowadays, the cost of solvent use has a non-negligible impact on production costs. Optimization of solvent ratios aims to improve reaction selectivity and yield and enhance byproduct treatment. In the future, it is expected that efficient and environmentally friendly alcoholysis solvents will be developed to achieve zero emission or high-value utilization, which will improve the economy and environmental friendliness. This paper focuses on the degradation of waste PIR by alcoholysis solvent ratios, hoping to provide a new idea for the degradation of waste PIR.

■ ASSOCIATED CONTENT

Supporting Information

The Supporting Information is available free of charge at https://pubs.acs.org/doi/10.1021/acsomega.4c07807.

Other experimental materials and photos of field tests (PDF)

■ AUTHOR INFORMATION

Corresponding Author

Xiaohua Gu − *School of Energy and Building Environment, Guilin University of Aerospace Technology, Guilin 541004, China; School of Material Science and Engineering, Qiqihar University, Qiqihar 161006, China; University Engineering Research Center of Green Upgrade Key Technology for Energy Industry, Guilin 541004, China;* orcid.org/0000-0001-9302-0374; Phone: +86-18115098088; Email: 2022049@guat.edu.cn

Authors

Qinglong Zhao − *College of Civil Engineering and Architecture, Northeast Petroleum University, Daqing 163318, China*

Shangwen Zhu − *School of Energy and Building Environment, Guilin University of Aerospace Technology, Guilin 541004, China;* orcid.org/0009-0008-0415-9445

Yan Liu − *School of Energy and Building Environment, Guilin University of Aerospace Technology, Guilin 541004, China; College of Civil Engineering and Architecture, Northeast Petroleum University, Daqing 163318, China*

Qingyong Su − *School of Energy and Building Environment, Guilin University of Aerospace Technology, Guilin 541004, China*

Complete contact information is available at: https://pubs.acs.org/10.1021/acsomega.4c07807

Notes

The authors declare no competing financial interest.

■ ACKNOWLEDGMENTS

The research was funded by the Scientific Research and Technology Development Program of Guilin (No. 20230120-9), Guilin Institute of Aerospace Technology Professor Fund Project (No. 2024BJXM018), Natural Science Foundation of Guangxi Province (No. 2024JJA160045), and the Guangxi Key Laboratory of Special Engineering Equipment and Control, Guilin University of Aerospace Technology (No. SEEC24ZR01), University Engineering Research Center of Green Upgrade Key Technology for Energy Industry, Guangxi (No. 202410-60).

■ REFERENCES

(1) Sair, S.; Oushabi, A.; Kammouni, A.; et al. Mechanical and thermal conductivity properties of hemp fiber reinforced polyurethane composites. *Case Stud. Constr. Mater.* **2018**, *8*, 203.

(2) Veronese, V. B.; Menger, R. K.; Forte, M. M. C.; Petzhold, C. L. Rigid polyurethane foam based on modified vegetable oil. *J. Appl. Polym. Sci.* **2011**, *120* (1), 530−537.

(3) Liu, S.; Wang, Q.; Sun, T.; Wu, C.; Shi, Y. The effect of different types of micro-bubbles on the performance of the coagulation flotation process for coke waste-water. *J. Chem. Technol. Biotechnol.* **2012**, *87* (2), 206−215.

(4) Kastek, M.; et al. Hyperspectral Imaging Infrared Sensor Used for Enviromental Monitoring. *Acta Phys. Polym. A* **2013**, *124* (3), 463−467.

(5) Lin, S.-H.; Gerber, D. J. Evolutionary energy performance feedback for design: Multidisciplinary design optimization and performance boundaries for design decision support. *Energy Build.* **2014**, *84*, 426−441.

(6) Xiaoyang, Z.; Zhi, C.; Shanlai, W.; Lei, Y.; Haitao, Y. High-Speed Temperature Control Method for MEMS Thermal Gravimetric Analyzer Based on Dual Fuzzy PID Control. *Micromachines* **2023**, *14* (5), No. 929.

(7) Guo, R.; Jacob, K. I. Effect of chain length distribution on thermal characteristics of model polytetrahydrofuran (PTHF) networks. *Polymer* **2014**, *55* (17), 4468−4477.

(8) Freeman, B.; Han, Y.; Hoogenboom, R.; Lutz, J. F.; Matyjaszewski, K. Frontiers in Polymer Science Editorial. *Polymer* **2024**, *299*, No. 126930.

(9) Sanders, D. F.; Guo, R.; Smith, Z. P.; Liu, Q.; Stevens, K. A.; McGrath, J. E.; Paul, D. R.; Freeman, B. D. Influence of polyimide precursor synthesis route and ortho -position functional group on thermally rearranged (TR) polymer properties: Conversion and free volume. *Polymer* **2014**, *55* (7), 1636−1647.
(10) Balgude, D.; Sabnis, A.; Ghosh, S. K. Synthesis and characterization of cardanol based aqueous 2K polyurethane coatings. *Eur. Polym. J.* **2016**, *85*, 620−634.
(11) Yaofa, L.; Hui, W.; Haibo, W.; Xu, C.; Zongliang, D. Enhanced flame retardancy and mechanical properties of waterborne polyurethane based on the phosphorus and nitrogen containing polybutadiene acrylonitrile. *J. Appl. Polym. Sci.* **2020**, *138* (20), No. 50432.
(12) Xin, J.; Xiaoyun, L.; Yali, D.; Yuhua, Z.; Junwei, W.; Maoqing, K.; Qifeng, L. Effect of the amide units in soft segment and urea units in hard segment on microstructures and physical properties of polyurethane elastomer. *Polymer* **2021**, *233*, No. 124205.
(13) Muralidharan, N. M.; Seema, A. Thermally Reduced Graphene oxide/thermoplastic Polyurethane Nanocomposites As Photomechanical Actuators. *Adv. Mater. Lett.* **2013**, *4* (12), 927−932.
(14) Junhuai, X.; Hui, W.; Xiaosheng, D.; Xu, C.; Zongliang, D.; Haibo, W. Self-healing, anti-freezing and highly stretchable polyurethane ionogel as ionic skin for wireless strain sensing. *Chem. Eng. J.* **2021**, *426*, No. 130724.
(15) Li, J.; Weiming, Y.; Zhao, N.; Bin, Y.; Yanning, Z. Sustainable Polyurethane Networks Based on Rosin with Reprocessing Performance. *Polymers* **2021**, *13* (20), 3538.
(16) Danae, V.; Pablo, F.; Evgenia, S.; Andrés, V.; Ricardo, C. S.; Raquel, V.; Alan, L.-M. M.; Héctor, A.-B. Effect of terbium(III) species on the structure and physical properties of polyurethane (TPU). *Polymer* **2021**, *233*, No. 124209.
(17) Changjiang, Y.; Martina, S. L.; Angela, M.; Corinna, P.; Ilaria, E.; Fabio, S.; Zhanhua, W.; Xi, Z.; Hesheng, X.; Marino, L. NIR light-triggered self-healing waterborne polyurethane coatings with polydopamine-coated reduced graphene oxide nanoparticles. *Prog. Org. Coat.* **2021**, *161*, No. 106499.
(18) Quan, H.; Zengfeng, W.; Qing, L.; Shiwei, L.; Lijie, N. Effects of Heterogeneous Linear Polyether Segments on the Membrane Breathability of Nonionic Polyurethane. *J. Macromol. Sci., Part B* **2021**, *60* (11), 914−927.
(19) Hu, W.; Wang, B.; Wang, X.; Ge, H.; Song, L.; Wang, J.; Hu, Y. Effect of ethyl cellulose microencapsulated ammonium polyphosphate on flame retardancy, mechanical and thermal properties of flame retardant poly(butylene succinate) composites. *J. Therm. Anal. Calorim.* **2014**, *117* (1), 27−38.
(20) Husainie, S. M.; Ullah, K. S.; Jason, R.; Ern, N. H. A Comparative Study on the Mechanical Properties of Different Natural Fiber Reinforced Free-Rise Polyurethane Foam Composites. *Ind. Eng. Chem. Res.* **2020**, *59* (50), 21745−21755.
(21) Kong, Z.; Ying, W. B.; Hu, H.; Wang, K.; Chen, C.; Tian, Y.; Li, F.; Zhang, R. Formation of crystal-like structure and effective hard domain in a thermoplastic polyurethane. *Polymer* **2020**, *210*, No. 123012.
(22) Yanbei, H.; Can, L.; Shuilai, Q.; Zhoumei, X.; Xiaowei, M.; Zhou, G.; Lei, S.; Yuan, H.; Weizhao, H. Preparation of soybean root-like CNTs/bimetallic oxides hybrid to enhance fire safety and mechanical performance of thermoplastic polyurethane. *Chem. Eng. J.* **2022**, *428*, No. 132338.
(23) Liu, Y.; Wenli, B.; Xiaoming, Z. The study on the electromagnetic properties of polyurethane coated pre-oxidized fiber felt composites. *J. Text. Inst.* **2021**, *112* (10), 1596−1601.
(24) Bagheri, A.; Jin, J. Photopolymerization in 3D Printing. *ACS Appl. Polym. Mater.* **2019**, *1* (4), 593−611.
(25) Sun, C.; Wang, Z.; Wang, Q.; Cao, J.; Li, W.; Tan, H.; Zhang, Y. Characterization of Polyurethane/Montmorillonite Nanocomposites: Morphology and Thermodynamics. *J. Polym. Environ.* **2020**, *29*, 1460−1466.
(26) van Hurne, S.; Raut, S. K.; Smulders, M. M. J. Recyclable Covalent Adaptable Polystyrene Networks Using Boronates and TetraAzaADamantanes. *ACS Appl. Polym. Mater.* **2024**, *6* (13), 7918−7925.
(27) Uram, K.; Maria, K.; Jacek, A.; Aleksander, P. Rigid Polyurethane Foams Modified with Biochar. *Materials* **2021**, *14* (19), 5616.
(28) Lu, Z.; Weilan, X.; Zuoxiang, Z.; Zhiyuan, Z. Synthesis and properties of reactive polyurethane hot melt adhesive based on a novel phosphorus-nitrogen-containing polyol. *J. Adhes. Sci. Technol.* **2021**, *35* (9), 941−954.
(29) Ding, H.; Quansheng, S.; Yanqi, W.; Dongzhe, J.; Chunwei, L.; Ce, J.; Yuping, F. Flexural Behavior of Polyurethane Concrete Reinforced by Carbon Fiber Grid. *Materials* **2021**, *14* (18), 5421.
(30) Ui, H. J.; Hee, L. T.; Daegeun, O.; Hyun-jong, P.; Man, N. S. Scratch-healable automotive clearcoats based on disulfide polyacrylate urethane networks. *Prog. Org. Coat.* **2021**, *161*, No. 106472.
(31) Tiuc, A. E.; Ovidiu, N.; Horatiu, V.; Tamas, G. D. R.; Ovidiu, V. New Sound Absorbing Materials Obtained from Waste Rigid Polyurethane Foam. *Mater. Plast.* **2019**, *56* (4), 1021−1027.
(32) Liu, H.; Bi, Z.; Wan, Z.; Wang, X.; Wan, Y.; Guo, X.; Cai, Z. Preparation and Performance Optimization of Two-Component Waterborne Polyurethane Locomotive Coating. *Coatings* **2020**, *10* (1), 4.
(33) Liu, S.; Yuan, W.; Di, F. Influence of polyurethane foam on chemical clogging of nonwoven geotextile and tailings caused by ferrous iron. *Text. Res. J.* **2021**, *91* (9−10), 1094−1103.
(34) Xu, Y.; Tang, L.; Iangthong, C. N.; Wagner, M.; Baumann, G.; Feist, F.; Bismarck, A.; Jiang, Q. Functionally Gradient Macroporous Polymers: Emulsion Templating Offers Control over Density, Pore Morphology, and Composition. *ACS Appl. Polym. Mater.* **2024**, *6* (9), 5150−5162.
(35) Caglayan, C.; Osken, I.; Ataalp, A.; Turkmen, H. S.; Cebeci, H. Impact response of shear thickening fluid filled polyurethane foam core sandwich composites. *Compos. Struct.* **2020**, *243*, 112171.
(36) Duan, N.; Sun, Z.; Ren, Y.; Liu, Z.; Liu, L.; Yan, F. Imidazolium-based ionic polyurethanes with high toughness, tunable healing efficiency and antibacterial activities. *Polym. Chem.* **2020**, *11* (4), 867−875.
(37) Wen, J.; Sun, Z.; Xiang, J.; Fan, H.; Chen, Y.; Yan, J. Preparation and characteristics of waterborne polyurethane with various lengths of fluorinated side chains. *Appl. Surf. Sci.* **2019**, *494*, 610−618.
(38) Silva, S. A.; Zawadzki, S. F.; Barbosa, R. V.; Ramos, L. P. Epoxidized corn oil polyol-based composites polyurethane flexible foams, preparation, and characterization. *Ciência Natura* **2019**, *41*, No. e44.
(39) Yang, Z.; Hu, D.; Liu, T.; Xu, Z.; Zhao, L. Strategy for preparation of microcellular rigid polyurethane foams with uniform fine cells and high expansion ratio using supercritical CO 2 as blowing agent. *J. Supercrit. Fluids* **2019**, *153*, 104601.
(40) Armstrong, S.; Freeman, B.; Hiltner, A.; Baer, E. Gas permeability of melt-processed poly(ether block amide) copolymers and the effects of orientation. *Polymer* **2012**, *53* (6), 1383−1392.
(41) Yongqian, S.; Chuan, L.; Libi, F.; Yuezhan, F.; Yuancai, L.; Zixiao, W.; Minghua, L.; Zhixin, C. Highly efficient MXene/Nano-Cu smoke suppressant towards reducing fire hazards of thermoplastic polyurethane. *Composites, Part A* **2021**, *150*, No. 106600.
(42) Zhou, W.; Bo, C.; Jia, P.; Zhou, Y.; Zhang, M. Effects of Tung Oil-Based Polyols on the Thermal Stability, Flame Retardancy, and Mechanical Properties of Rigid Polyurethane Foam. *Polymers* **2019**, *11* (1), 45.
(43) Asadchikov, V. E.; et al. X-ray Reflectometry of Thin Films Formed during Phase Separation of Organic Solutions of Aliphatic Polyethers in Water. *Crystallogr. Rep.* **2023**, *68* (1), 104−109.
(44) Kerche, E. F.; Avila, D. R.; Liberato, P. C.; Campos, A. S. Rigid bio-based wood/polyurethane foam composites expanded under confinement. *J. Cell. Plast.* **2021**, *57* (5), 757−768.
(45) Olmedo-Martínez, J. L.; Meabe, L.; Basterretxea, A.; Mecerreyes, D.; Müller, A. J. Effect of Chemical Structure and Salt

https://doi.org/10.1021/acsomega.4c07807
ACS Omega 2025, 10, 12917−12927

Concentration on the Crystallization and Ionic Conductivity of Aliphatic Polyethers. *Polymers* **2019**, *11* (3), 452.
(46) Xu, X.; Muyao, M.; Jiaxin, G.; Tongxin, S.; Yuhan, G.; Daming, F.; Lei, Z. Multifunctional Ni-NPC Single-Atom Nanozyme for Removal and Smartphone-Assisted Visualization Monitoring of Carbamate Pesticides. *Inorg. Chem.* **2024**, *63*, 1225−1235.
(47) Temizkan, E.; Gülden, E.; Ayça, E.; Hüseyin, D. Preparation, characterization, and influence of polyurea coatings on their layered composite materials based on flexible rebonded polyurethane. *Polym. Eng. Sci.* **2021**, *61* (5), 1392−1404.
(48) Khafagy, A. G.; Mahmoud, M. A. Polyurethane Versus Chitosan-Based Polymers Nasal Packs After Functional Endoscopic Sinus Surgery: A Prospective Randomized Double-Blinded Study. *Am. J. Rhinol. Allergy* **2021**, *35* (5), 624−630.
(49) Kumar, D.; Anil, B. S.; Navin, K.; Prashant, J. Two-step synthesis of polyurethane/multi-walled carbon nanotubes polymer composite to achieve high percentage particle reinforcement for mechanical applications. *J. Compos. Mater.* **2021**, *55* (21), 2877−2885.
(50) Troels, R.; Irakli, J.; Seonghyeon, J.; Katja, J.; Seunghwan, L. Low friction thermoplastic polyurethane coatings imparted by surface segregation of amphiphilic block copolymers. *Colloid Interface Sci. Commun.* **2021**, *44*, No. 100477.
(51) Olivieri, F.; Fabio, S.; Rachele, C.; Mariacristina, C.; Antonino, S.; Gennaro, G.; Marino, L. Effectiveness of Mesoporous Silica Nanoparticles Functionalized with Benzoyl Chloride in pH-Responsive Anticorrosion Polymer Coatings. *ACS Appl. Polym. Mater.* **2023**, *5* (8), 5917−5925.

https://doi.org/10.1021/acsomega.4c07807
ACS Omega 2025, 10, 12917−12927